ESE-ENDOR and ESEEM Characterization of Water and Methanol Ligation to a Dinuclear Mn(III)Mn(IV) Complex†

David W. Randall,‡ Andrew Gelasco,§ M. Tyler Caudle,§ Vincent L. Pecoraro,*,§ and R. David Britt*,‡

Contribution from the Department of Chemistry, University of California, Davis, California 95616-0935, and Department of Chemistry, University of Michigan, Ann Arbor, Michigan 48109-1055

Received October 23, 1996⊗

Abstract: Interactions of water and methanol with a mixed valence Mn(III)Mn(IV) complex are explored with ^{1}H electron spin echo (ESE)-electron nuclear double resonance (ENDOR) and ^{1}H and ^{2}H ESE envelope modulation (ESEEM). Derivatives of the (2-OH-3,5-Cl_2-SALPN)$_2$ Mn(III)Mn(IV) complex are ideal for structural and spectroscopic modeling of water binding to multinuclear Mn complexes in metalloproteins, specifically photosystem II (PSII) and manganese catalase (MnCat). Using ESE-ENDOR and ESEEM techniques, ^{1}H hyperfine parameters are determined for both water and methanol ligated to the Mn(III) ion of the complex. The protons of water directly bound to Mn(III) are inequivalent and exhibit roughly axial dipolar hyperfine interactions (T_{dip} = 8.4 MHz and T_{dip} = 7.4 MHz), permitting orientations and radial distances to be determined using a model where the proton experiences a point dipole interaction with each Mn ion. General equations are given for the components of the rhombic dipolar hyperfine interaction between a proton and a spin coupled dinuclear metal cluster. The observed ENDOR pattern is from water protons 2.65 and 2.74 Å from the Mn(III) which make an Mn(IV)−Mn(III)−H angle of ∼160°. For the alcohol proton in the analogous methanol bound complex, a 2.65 Å Mn(III)−H distance is observed. Three pulse ^{2}H ESEEM gives best fit Mn(III)−^{2}H(^{1}H) radial distances of 3.0, 3.5, and 4.0 Å for the three methyl deuterons in this complex.

Introduction

Mixed-valence multinuclear manganese complexes have been synthesized for many years, (reviewed in refs 1−6) in part with the purpose of providing spectroscopic and structural models for multinuclear manganese enzymes, including manganese catalase (MnCat) and the oxygen evolving complex (OEC) of Photosystem II (PSII). Both of these enzymes are of considerable biological importance: manganese catalase disproportionates H_2O_2 to H_2O and O_2,[7,8] while the OEC oxidizes H_2O to O_2.[9−11] X-ray absorption experiments on these enzyme systems implicate high valence Mn atoms separated by distances as short as 2.7 Å in the OEC[12−14] and in a super-oxidized form of MnCat (MnCat(III,IV)).[15] Such high valence Mn complexes are often modeled with small synthetic complexes containing Mn(III)-Mn(IV) valence trapped bis-μ-oxo cores with similar Mn−Mn distances. The ligation environments of the enzymatic metal complexes are crucial to enzymatic function. In particular, water is a ligated substrate of the OEC in PSII,[9−11,16] and water has also been proposed to be a ligand to MnCat in some oxidation states. Small alcohols (e.g., methanol and ethanol) are substrate analogs for PSII which bind to the Mn cluster.[17]

EPR spectroscopy has been an important tool for probing the electronic environment of the manganese ions in these complexes. EPR spectra have been reported for the biological systems[18−20] and model compounds.[21−31] Manganese hyperfine interactions of the 100% abundant ^{55}Mn nucleus with the

† Keywords: pulsed EPR, mixed-valence manganese, water ligation, dipolar hyperfine interaction.

‡ University of California.

§ University of Michigan.

⊗ Abstract published in *Advance ACS Abstracts,* May 1, 1997.

(1) Riggs-Gelasco, P. J.; Stemmler, T. L.; Penner-Hahn, J. E. *Coord. Chem. Rev.* **1995**, *144*, 245−286.

(2) Manchandra, R.; Brudvig, G. W.; Crabtree, R. H. *Coord. Chem. Rev.* **1995**, *144*, 1−38.

(3) Armstrong, W. H. In Manganese Redox Enzymes; Pecoraro, V. L., Ed.; VCH Publishers: New York, 1992; pp 261−286.

(4) Pecoraro, V. L.; Baldwin, M. J.; Gelasco, A. *Chem. Rev.* **1994**, *94*, 807−826.

(5) Christou, G. *Acc. Chem. Res.* **1989**, *22*, 328−335.

(6) Wieghardt, K. *Angew. Chem.* **1989**, *101*, 1179−98.

(7) Penner-Hahn, J. E. In *Manganese Redox Enzymes*; Pecoraro, V. L., Ed.; VCH Publishers: New York, 1992; pp 29−45.

(8) Dismukes, G. C. In *Bioinorganic Catalysis*; Reedijk, J., Ed.; Marcel Dekker: New York, 1993; pp 317−346.

(9) Debus, R. J. *Biochim. Biophys. Acta* **1992**, *1102*, 269−352.

(10) Britt, R. D. In *Oxygenic Photosynthesis: The Light Reactions*; Ort, D. R., Yocum, C. F., Eds.; Kluwer Academic: Dordrecht, The Netherlands, 1996; pp 137−164.

(11) Hoganson, C. W.; Babcock, G. T. In *Metal Ions in Biological Systems: Metalloenzymes Involving Amino Acid-Residue and Related Radicals*; Sigel, H., Sigel, A., Eds.; Marcel Dekker, Inc: New York, 1994; pp 77−107.

(12) Penner-Hahn, J. E.; Fronko, R. M.; Pecoraro, V. L.; Yocum, C. F.; Betts, S. D.; Bowlby, N. R. *J. Am. Chem. Soc.* **1990**, *112*, 2549−2557.

(13) Yachandra, V. K.; Derose, V. J.; Latimer, M. J.; Mukerji, I.; Sauer, K.; Klein, M. P. *Science* **1993**, *260*, 675−679.

(14) George, G. N.; Prince, R. C.; Cramer, S. P. *Science* **1989**, *243*, 789−791.

(15) Waldo, G. S.; Yu, S. Y.; Penner-Hahn, J. E. *J. Am. Chem. Soc.* **1992**, *114*, 5869−5870.

(16) Gilchrist, M. L.; Randall, D. W.; Ball, J. A.; Britt, R. D. Manuscript in preparation.

(17) Force, D. A.; Lorigan, G. A.; Randall, D. W.; Clemens, K.; Britt, R. D. Manuscript in preparation.

(18) Dismukes, G. C.; Siderer, Y. *Proc. Natl. Acad. Sci. U.S.A.* **1981**, *78*, 247−278.

(19) Khangulov, S. V.; Voyevodskaya, N. V.; Varynin, V. V.; Grebenko, A. I.; Melik-Adamyan, V. R. *Biofizica* **1987**, *32*, 1044−1051.

(20) Fronko, R. M.; Penner-Hahn, J. E.; Bender, C. J. *J. Am. Chem. Soc.* **1988**, *110*, 7554−7555.

(21) Cooper, S. R.; Dismukes, G. C.; Klein, M. P.; Calvin, M. *J. Am. Chem. Soc.* **1978**, *100*, 7248−7252.

(22) Brewer, K. J.; Calvin, M.; Lumpkin, R. S.; Otvos, J. W.; Spreer, L. O. *Inorg. Chem.* **1989**, *28*, 4446−4451.

(23) Buchanan, R. M.; Oberhausen, K. J.; Richardson, J. F. *Inorg. Chem.* **1988**, *27*, 971−973.

(24) Camenzind, M. J.; Schardt, B. C.; Hill, C. L. *Inorg. Chem.* **1984**, *23*, 1984−1986.

S0002-7863(96)03682-7 CCC: $14.00

strongly antiferromagnetically exchange coupled electron spins of the Mn ions dominate the EPR spectra of these complexes.[21,32−34] ^{55}Mn ESE-ENDOR experiments on PSII and model compounds have revealed information about the ^{55}Mn hyperfine and ^{55}Mn quadrupolar couplings and also confirmed the presence of a tetranuclear Mn cluster in the OEC of PSII.[10,35] To describe the $S = 1/2$ ground spin state EPR spectra of these strongly antiferromagnetically exchange coupled *n*-nuclei clusters, a spin Hamiltonian in the coupled representation is appropriate:[21,36]

$$H = \beta_e \hat{\vec{S}}_T \cdot \tilde{\mathbf{g}} \cdot \vec{B} + \sum_{i=1,n} \hat{\vec{S}}_T \cdot \tilde{\mathbf{A}}_i \cdot \hat{\vec{I}}_i \qquad (1)$$

where β_e is the Bohr magneton, $\hat{\vec{S}}_T$ is the total electronic spin operator, the $\tilde{\mathbf{g}}$ matrix describes the interaction between the electronic spin and the magnetic field $\vec{B}$, $\vec{I}$ is the nuclear spin operator, and $\tilde{\mathbf{A}}$ is the effective hyperfine interaction matrix.

The considerable line widths of the ^{55}Mn EPR powder patterns of these complexes preclude resolution of superhyperfine interactions from magnetic ligand nuclei unless the higher resolution techniques of electron nuclear double resonance (ENDOR) and/or electron spin echo envelope modulation (ESEEM) are used.[37] The superhyperfine interactions give insight into ligand orientation and interactions with these antiferromagnetically exchange coupled manganese clusters. Ligand interactions in the biological systems have been probed by ^{1}H, ^{14}N, and ^{15}N ENDOR[16,38−40] and ^{2}H, ^{14}N, and ^{15}N ESEEM[16,17,41−45] with considerable success. ESEEM and ENDOR experiments performed on model compounds[39,40,46−50] have probed ^{14}N and nonwater ^{1}H interactions with the Mn(III)-Mn(IV) core. Though crystal structures exist for model complexes containing water directly bound to manganese,[51,52] magnetic resonance techniques capable of exploring water proton−dinuclear manganese complex interactions (ENDOR and ESEEM) have not been applied, until now, to these systems, in spite of the considerable biological relevance.

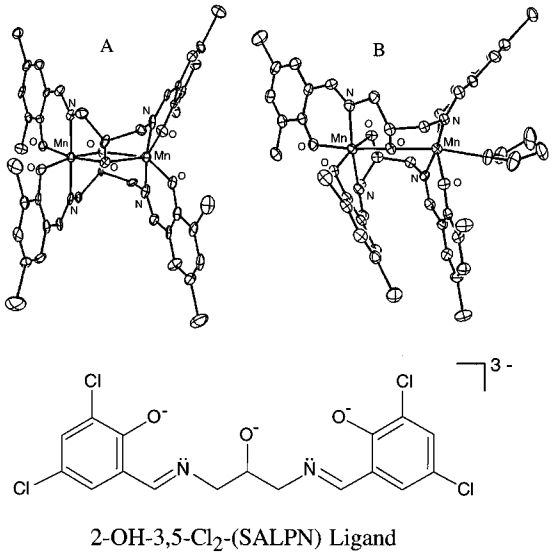

Figure 1. Crystal structures of **1** and **1** + THF. Adapted from refs 53 and 54.

In this paper we use advanced EPR methods to explore the geometries of such biologically relevant ligands with respect to a dinuclear Mn complex utilizing a set of solvent−ligated complexes derived from the symmetric (2-OH-3,5-Cl_2-SALPN)$_2$ Mn(III)Mn(IV) complex **1**.[53−55] In solutions containing **1** and an electron donating solvent such as water, THF, or methanol, dinuclear Mn(III)Mn(IV) complexes are formed in which the solvent is directly ligated to the Mn(III) ion.[53] Representations of the molecular structures determined from X-ray crystallography on **1** and **1** + THF are presented in Figure 1 along with the 2-OH-SALPN ligand. Two μ-alkoxo moieties bridge the antiferromagnetically coupled Mn ions in **1**. With the solvent-ligand (e.g., water, THF, or methanol) binding along the Jahn−Teller distorted axis of Mn(III) to make **1** + ligand, the symmetry is reduced by breaking one of the μ-alkoxo bridges. Complex **1**, with or without ligated solvent-ligands, differs from μ-oxo bridged Mn(III)Mn(IV) model complexes (e.g., bipyridyl ligated). The Mn−Mn distance is significantly

(25) Diril, H.; Chang, H.-R.; Nilges, M. J.; Zhang, X.; Potenza, J. A.; Schugar, H. J.; Isied, S. S.; Hendrickson, D. N. *J. Am. Chem. Soc*. **1989**, *111*, 5102−5114.
(26) Goodson, P. A.; Hodgson, D., J.; Glerup, J.; Michelsen, K.; Weihe, H. *Inorg. Chim. Acta* **1992**, *197*, 141−147.
(27) Hagen, K. S.; Armstrong, W. H.; Hope, H. k. *Inorg. Chem*. **1988**, *27*, 967−969.
(28) Perrée-Fauvet, M.; Gaudemer, A.; Bonvoisin, J.; Girerd, J. J.; Boucly-Goester, C.; Boucly, P. *Inorg. Chem*. **1989**, *28*, 3533−3538.
(29) Schake, A. R.; Schmitt, E. A.; Conti, A. J.; Streib, W. E.; Huffman, J. C.; Hendrickson, D. N.; Christou, G. *Inorg. Chem*. **1991**, *30*, 3192−3199.
(30) Sheats, J. E.; Czernuszewicz, R. S.; Dismukes, G. C.; Rheingold, A. L.; Petrouleas, V.; Stubbe, J.; Armstrong, W. H.; Beer, R. H.; Lippard, S. J. *J. Am. Chem. Soc*. **1987**, *109*, 1435−1444.
(31) Wieghardt, K.; Bossek, U.; Zsolnai, L.; Huttner, G.; Blondin, G.; Girerd, J.-J.; Babonneau, F. *J. Chem. Soc., Chem. Commun.* **1987**, 651−653.
(32) Haddy, A.; Waldo, G. S.; Sands, R. H.; Penner-Hahn, J. E. *Inorg. Chem*. **1994**, *33*, 2677−2682.
(33) Zheng, M.; Khangulov, S. V.; Dismukes, G. C.; Barynin, V. V. *Inorg. Chem*. **1994**, *33*, 382−387.
(34) Zheng, M.; Dismukes, G. C. *Inorg. Chem.* **1996**, *35*, 3307−3319.
(35) Randall, D. W.; Sturgeon, B. E.; Ball, J. A.; Lorigan, G. A.; Chan, M. K.; Klein, M. P.; Armstrong, W. H.; Britt, R. D. *J. Am. Chem. Soc*. **1995**, *117*, 11780−11789.
(36) Bencini, A.; Gatteschi, D. *Electron Paramagnetic Resonance of Exchange Coupled Systems*; Springer-Verlag: Berlin, 1989; pp 48−66.
(37) In the tetrakis 2,2′ bipyridyl (bipy) ligated $[Mn_2O_2]^{3+}$ core, to ^{14}N to ^{15}N isotopic ligand substitution reveals no change in the CW-EPR spectra, demonstrating that the major portion of the EPR transition line widths are intrinsic to the ^{55}Mn EPR powder patterns.[49]
(38) Kawamori, A.; Inui, T.; Ono, T.; Inoue, Y. *FEBS Lett*. **1989**, *254*, 219−224.
(39) Tang, X. S.; Sivaraja, M.; Dismukes, G. C. *J. Am. Chem. Soc*. **1993**, *115*, 2382−2389.
(40) Khangulov, S.; Sivaraja, M.; Barynin, V. V.; Dismukes, G. C. *Biochemistry* **1993**, *32*, 4912−4924.
(41) Dikanov, S. A.; Tsvetkov, Y. D.; Khangulov, S. V.; Goldfeld, M. G. *Dokl. Biophys*. **1988**, *302*, 174−177.
(42) Ivancich, A.; Barynin, V. V.; Zimmermann, J. L. *Biochemistry* **1995**, *34*, 6628−6639.
(43) Tang, X.-S.; Gilchrist, M. L.; Lorigan, G. A.; Larson, B.; Britt, R. D.; Diner, B. A. *Proc. Natl. Acad. Sci. U.S.A.* **1994**, *91*, 704−708.
(44) Zimmermann, J.-L.; Boussac, A.; Rutherford, A. W. *Biochemistry* **1993**, *32*, 4931−4841.
(45) Stemmler, T. L.; Sturgeon, B. E.; Randall, D. W.; Britt, R. D.; Penner-Hahn, J. E. Submitted to *J. Am. Chem. Soc.*
(46) Tan, X.; Gultneh, Y.; Sarneski, J. E.; Scholes, C. P. *J. Am. Chem. Soc*. **1991**, *113*, 7853−7858.
(47) Zweygart, W.; Thanner, R.; Lubitz, W. *J. Magn. Reson. Ser. A* **1994**, *109*, 172−176.
(48) Britt, R. D. Ph.D. Thesis, Department of Physics, Lawrence Berkeley Laboratory, University of California, Berkeley, 1988.
(49) Sturgeon, B. E. Ph.D. Thesis, Department of Chemistry, University of California, Davis, 1994.
(50) Britt, R. D.; Sturgeon, B. E.; Randall, D. W.; Chan, M. K.; Klein, M. P.; Armstrong, W. H. Manuscript in preparation.
(51) Bossek, U.; Saher, M.; Weyhermüller, T.; Wieghardt, K. *J. Chem. Soc., Chem. Commun*. **1992**, 1780−1782.
(52) Suzuki, M.; Hayashi, Y.; Munezawa, K.; Suenaga, M.; Senda, H.; Uehara, A. *Chem. Lett*. **1991**, 1929−1932.
(53) Larson, E.; Haddy, A.; Kirk, M. L.; Sands, R. H.; Hatfield, W. E.; Pecoraro, V. L. *J. Am. Chem. Soc*. **1992**, *114*, 6263−6265.
(54) Gelasco, A.; Kirk, M. L.; Kampf, J. W.; Pecoraro, V. L. submitted to *Inorg. Chem*.
(55) SALPN is *N*,*N*′-bissalicylidene-1,3-diamino-2-hydroxypropane (see Figure 1).

longer (3.32 Å in **1**,[54] 3.65 Å in **1** + THF[53]) compared to ~2.7 Å in bis-μ-oxo bridged model compounds.[2,6] The geometry differences between the μ-alkoxo and μ-oxo bridged complexes affect a greater than 10-fold reduction in the exchange coupling constant, J ($J_1 \approx -2$ cm^{-1})[54] compared to that observed in complexes containing μ-oxo (and acetato) bridges ($|J| \geq 100$ cm^{-1}).[2,6] The small J value of **1** and its solvent-ligand bound derivatives yields strongly temperature dependent EPR spectra. A ~12 line EPR pattern at $g = 2$ is observed at 4.2 K. Spectroscopic features attributed to thermally populated excited spin states are observed at higher g value ($g \geq 4$) with increasing temperature.[53] Zheng *et al.*[33] interpret the unusual ~12 line EPR pattern by invoking frequently neglected terms in perturbation theory equations describing the effective ^{55}Mn hyperfine interaction matrix ($\tilde{\mathbf{A}}$) observed in exchange coupled systems Mn(III)Mn(IV) (*vide infra*). Such interactions have been frequently utilized in magnetic studies of dinuclear non-heme iron proteins.[56−58]

We have performed ENDOR and ESEEM studies of both water and methanol ligation to the μ-alkoxo bridged Mn(III)-Mn(IV) complex. Analysis of the ^{1}H ENDOR and ESEEM spectra for water bound to Mn(III) in the μ-alkoxo bridged Mn(III)Mn(IV) core using a model where the proton experiences a dipolar interaction with spin coupled Mn ions[39,40,56] provides an accurate measure of the distance between protons on the ligated water and the Mn(III) as well as some measure of their relative orientation. Equations for the components of the dipolar hyperfine interaction described in this model are presented. The alcohol proton in methanol is found to assume a similar geometry to the bound water protons. Interactions of methyl deuterons (protons) in methanol bound to the μ-alkoxo core are probed by three pulse ESEEM to established distances and orientation with respect to the Mn(III)Mn(IV) core. This analysis of ligand interactions with the well-defined manganese core of this model compound provides a basis for parallel analyses of water[16] and alcohol[17] ligation to the Mn cluster in PSII.

ENDOR and ESEEM Background. In cases where superhyperfine coupling is not resolved in the EPR spectrum, ENDOR and ESEEM can determine hyperfine coupling interactions which can be interpreted to yield structural information.[59−61] In general, both techniques monitor nuclear magnetic spin transitions of nuclei coupled to electrons. In the ENDOR experiment, changes in the EPR amplitude are recorded as incident RF power is incremented in an appropriate range to drive nuclear magnetic spin transitions.[60−62] In an ESEEM experiment, the electron spin echo (ESE) amplitude is observed as a function of interpulse time in a spin echo pulse sequence. The ESE is modulated at frequencies which depend on the nature and magnitude of the electron-nuclear interaction. The depth of the modulation depends on the amount of quantum mechanical state mixing within the coupled electron-nuclear system.[63]

The relevant nuclear spin Hamiltonian for a system with both electron and nuclear spins of 1/2 ($S = 1/2$, $I = 1/2$) is comprised of the (super) hyperfine interaction and the nuclear Zeeman interaction:[64,65]

$$H = H_{\mathrm{HF}} + H_{\mathrm{n.Z}} \tag{2}$$

$$H = \hat{\vec{S}} \cdot \tilde{\mathbf{A}} \cdot \hat{\vec{I}} - \beta_N \hat{\vec{I}} \cdot \tilde{\mathbf{g}}_{\mathbf{N}} \cdot \vec{B} \tag{3}$$

The nuclear Zeeman interaction is isotropic and analogous to the electronic Zeeman interaction. The hyperfine interaction depends on the coupling between the unpaired electron and surrounding magnetic nuclei. In matrix notation it is described as the sum of isotropic and dipolar (anisotropic) matrices

$$\tilde{\mathbf{A}} = A_{\mathrm{iso}}\tilde{\mathbf{1}} + \tilde{\mathbf{A}}_{\mathrm{dip}} \tag{4}$$

where $\tilde{\mathbf{1}}$ is a unit matrix and A_{iso} is the isotropic Fermi-contact interaction due to unpaired electron density at the coupled nucleus. The second contribution to the hyperfine (eq 4) is an anisotropic dipole−dipole interaction between the spin of the unpaired electron ($\vec{S}$) and the spin of the coupled nucleus ($\vec{I}$). The magnitude of this interaction varies as $1/r^3$, where r is the distance between the unpaired electron and the nucleus. A principal axis system exists where the dipolar portion ($\tilde{\mathbf{A}}_{\mathrm{dip}}$) has no off-diagonal terms and is traceless with components A^d_{xx}, A^d_{yy}, and A^d_{zz} along orthogonal axes. The interaction between two such point dipoles isolated from other magnetic dipoles has axial symmetry. In this common situation, two components of the interaction matrix are equal while the third is twice as large but opposite in sign (i.e., $A^d_{xx} = A^d_{yy} = -1/2A^d_{zz}$). In this situation, the components of the dipolar hyperfine interaction matrix ($\tilde{\mathbf{A}}_{\mathrm{dip}}$) depend on a single parameter denoted $T_{\mathrm{dip}} = -A^d_{xx} = -A^d_{yy}$ which depends on the radial distance between the coupled electronic and nuclear spins. For this case the dipolar hyperfine interaction, $\tilde{\mathbf{A}}_{\mathrm{dip}}$, can be written as

$$\tilde{\mathbf{A}}_{\mathrm{dip}} = T_{\mathrm{dip}}\tilde{\Delta} = \frac{g_e \beta_e g_N \beta_N}{hr^3}\begin{pmatrix} -1 & 0 & 0 \\ 0 & -1 & 0 \\ 0 & 0 & 2 \end{pmatrix} \tag{5}$$

where g_e, β_e, g_N, and β_N are the respective electronic and proton nuclear g-factors and magnetons.[65] To the extent that a metal ion is approximated by a point charge, the radial distance (r) between the electronic and coupled nuclear spins is determined from T_{dip}:

$$r = [g_e g_N \beta_e \beta_N / (hT_{\mathrm{dip}})]^{1/3} \tag{6}$$

For a spin $I \geq 1$ nucleus, a nuclear quadrupolar interaction ($\hat{\vec{I}} \cdot \tilde{\mathbf{P}} \cdot \hat{\vec{I}}$) must be added to equation 3. The small quadrupole moment of the $I = 1$ deuterium nucleus (^{2}H) typically broadens ^{2}H ENDOR or ESEEM peaks, though well resolved quadrupolar structure is reported in some cases.[60,66] In situations where the electronic magnetic moment is distributed between two metal atoms as in **1**, a more complex analysis is required, because

(56) DeRose, V. J.; Liu, K. E.; Lippard, S. J.; Hoffman, B. M. *J. Am. Chem. Soc.* **1996**, *118*, 121−134.
(57) Fox, B. G.; Hendrich, M. P.; Surerus, K. K.; Andersson, K. K.; Froland, W. A.; Lipscomb, J. D.; Münck, E. *J. Am. Chem. Soc.* **1993**, *115*, 3688−3701.
(58) Sage, J. T.; Xia, Y.-M.; Debrunner, P. G.; Keough, D. T.; de Jersey, J.; Zerner, B. *J. Am. Chem. Soc.* **1989**, *111*, 7239−7247.
(59) Britt, R. D. In *Biophysical Techniques in Photosynthesis*; Amesz, J., Hoff, A. J., Eds.; Kluwer Academic: Dordrecht, The Netherlands, 1996; pp 235−253.
(60) Hoffman, B. M.; DeRose, V. J.; Doan, P. E.; Gurbiel, R. J.; Houseman, A. L. P.; Telser, J. In *Biological Magnetic Resonance*; Berliner, L. J., Reuben, J., Eds.; Plenum Press: New York, 1993; pp 151−218.
(61) Thomann, H.; Bernardo, M. In *Methods in Enzymology*; Riordan, J. F., Vallee, B. L., Eds.; Academic Press: San Diego, 1993; pp 118−189.
(62) Gemperle, C.; Schweiger, A. *Chem. Rev.* **1991**, *91*, 1491−1505.
(63) Dikanov, S. A.; Tsvetkov, Y. D. *Electron Spin Echo Envelope Modulation (ESEEM)*; CRC Publishers: Boca Raton, FL, 1993.
(64) Kevan, L.; Kispert, L. *Electron Spin Double Resonacne Spectroscopy*; John Wiley & Sons: New York, 1976; pp 165−175.
(65) Weltner, W., Jr. *Magetic Atoms and Molecules*; Dover Publications, Inc.: New York, 1983; 52−57.
(66) Force, D. A.; Randall, D. W.; Britt, R. D.; Tang, X.-S.; Diner, B. A. *J. Am. Chem. Soc.* **1995**, *117*, 12643−12644.

the proton will experience a dipolar interaction with the unpaired electron spin density on both metal atoms (*vide infra*).

Experimental Section

Samples and Synthesis. Compound **1** was prepared by the method described previously.[53, 54] Various solvent adducts of **1** were prepared by the addition of isotopically labeled solvents. The following solvent-ligands were used: ^1H_2O (double deionized); ^2H_2O (Cambridge Isotope Labs, 99.8% isotopic purity); CH_3OH (Fisher, natural abundance); CD_3-OD (Aldrich, 99.8% isotopic purity); and CH_3OD (Aldrich, 99.5% isotopic purity). To prepare the complexes for EPR analysis, **1** was dissolved in acetonitrile (Mailinckrodt, analytical reagent grade), and an equal volume of dichloromethane (Fisher, certified ACS grade) was then added to the solution, followed by the addition of the solvent-ligand. The resulting samples were ~10 mM in Mn complex in a solvent system of 9:9:2 (CH_3CN:CH_2Cl_2:solvent−ligand). The OH^- ligated **1** was prepared by reacting [(2-OH-SALPN)$_2$Mn(III)$_2$] with 1.1 equiv of *tert*-butyl hydroperoxide in CH_2Cl_2 at −20 °C. Addition of 1 volume of heptane followed by evaporation of the CH_2Cl_2 at −20 °C afforded pure [(2-OH-SALPN)$_2$(OH)Mn(III)Mn(IV)] (i.e., **1**-OH) as shown by elemental analysis, UV−vis, EPR, and IR.[67] To obtain the O^1H^- and O^2H^- ligated compounds used for the ENDOR experiments, OH^- ligated **1** was incubated for 30 min at −30 °C in a solvent system of 9:9:2 CH_3CN:CH_2Cl_2:^1H_2O/^2H_2O. In all these samples, the solvent ligand was in >500-fold molar excess. After preparation, samples were placed in 3.8 mm OD precision quartz EPR tubes (Wilmad) and then immediately cooled to 77 K for storage.

Spectroscopy. ESE. The spin echo spectrometer used to perform the ESE-EPR, ESE-ENDOR, and ESEEM experiments has been described elsewhere.[66,68] All experiments were performed at X-band microwave frequencies with the sample immersed in liquid Helium (4.2 K). ESE-EPR field sweeps were recorded as the magnetic field dependence of the spin echo amplitude induced by a $\pi/2$-τ-π-echo pulse sequence, where π and $\pi/2$ indicate the turning angles of the microwave pulses. ESE-ENDOR experiments utilized the pulse sequence of Davies[69] (π-T-$\pi/2$-τ-π-echo).[60,61] In this sequence, RF power is applied during the time T to drive nuclear spin transitions. The pulsed nature of ESE-ENDOR is advantageous because contributions from matrix (distant) protons are minimized, and the ENDOR signal is detected in the absence of high RF and microwave power which often leads to baseline distortions in continuous wave (CW) ENDOR.[59−61] Two pulse ESEEM experiments were performed in the usual manner by observing the τ-dependence of the electron spin echo induced by the $\pi/2$-τ-π-echo pulse sequence.[70] Three pulse ESEEM experiments measure the T dependence of the stimulated echo amplitude from the $\pi/2$-τ-$\pi/2$-T-$\pi/2$-echo pulse sequence.[70] Frequency domain spectra were obtained from Fourier analysis of the time domain modulation patterns following the deadtime-backfill method described by Mims.[71]

CW-EPR. CW-EPR spectra were recorded using a Bruker ECS-106 spectrometer with a TE_{102} dual-mode cavity operated in the conventional perpendicular polarization mode ($B_1 \perp B_0$). The temperature was maintained at 4.2 K with an Oxford liquid He flow system (ESR900).

UV−visible. UV−visible spectra were measured on Perkin-Elmer Lambda 9 UV−vis-nearIR spectrophotometer equipped with a PE 3600 data station.

Results and Discussion

UV−visible. UV−visible electronic spectroscopy demonstrates that when prepared as described, the complexes exist with the solvent ligand bound to the Mn core. Water was added to a 1:1 acetonitrile:dichloromethane solution of the symmetric dimer [2-OH(3,5-Cl_2-SALPN) Mn(III)Mn(IV)] ClO_4 (i.e., **1**), and the conversion was monitored by electronic spectroscopy. Electronic spectra of **1** + 1000 equiv of H_2O (0.1% v/v), 30 000 equiv of H_2O (2.9% v/v), and 100 000 equivalents of H_2O (9% v/v) show the conversion to the asymmetric complex [{2-OH-(3,5-Cl_2-SALPN)}(H_2O) Mn(III)Mn(IV)] ClO_4 (i.e., **1** + ^1H_2O) (data not shown).[72,73] Further addition of water (up to 25%) showed no further change in the electronic spectra. Similar experiments with methanol as the exogenous ligand showed similar results with 10% methanol converting **1** to [{2-OH(3,5-Cl_2-SALPN)}(CH_3OH) Mn(III)Mn(IV)] ClO_4 (i.e., **1** + MeOH).

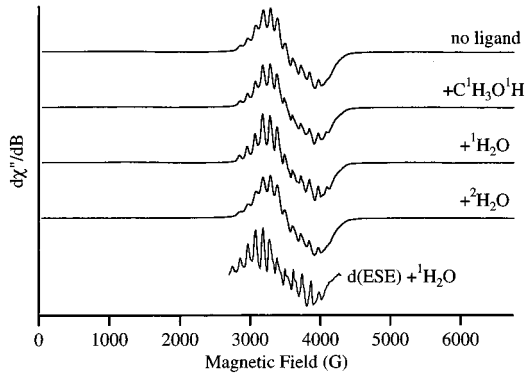

Figure 2. CW-EPR spectra of **1** with and without solvent-ligands. A numerical derivative of the ESE-EPR spectrum of the $+^1$ H_2O ligated complex is included for comparison and labeled d(ESE). The added ligands are labeled on the graph. Experimental CW-EPR parameters: ν_{MW} = 9.68 GHz; MW power = 2.0 mW; modulation amplitude = 5 G; modulation frequency = 100 kHz; temperature = 4.2 K; time constant = 10.24 ms; scan time = 84 sec. ESE-EPR parameters: ν_{MW} = 9.3738 GHz; τ = 400 ns; $\pi/2$ = 100 ns; MW power ≈ 2 W; repetition rate = 500 Hz; temperature = 4.2 K. The ESE-EPR derivative has been offset by 109 G to account for the field shift of $g = 2$ due to different microwave frequencies.

CW-EPR. The CW-EPR spectra of **1**, **1** + ^1H_2O, **1** + ^2H_2O, and **1** + MeOH at 4.2 K are shown in Figure 2 and are identical to those previously reported by Larson *et al.*[53] Little variation is observed in these spectra, requiring higher resolution techniques such as ENDOR and ESEEM to probe the ligand environment in these complexes. Also presented in Figure 2 is a numerical derivative of the ESE-EPR spectrum of **1** + ^1H_2O. Though the basic spectral features are similar, the numerical derivative of the ESE-EPR spectrum gives slightly better resolution than the CW-EPR spectra. In all cases, approximately 12 of the 36 EPR transitions[21,32,33,35] expected for an effective electron spin $S = 1/2$ coupled to two inequivalent ^{55}Mn nuclei ($I = 5/2$) are resolved. Anisotropy in the electronic Zeeman interaction ($\tilde{\mathbf{g}}$) and ^{55}Mn hyperfine interactions ($\tilde{\mathbf{A}}$) of the μ-alkoxo bridged systems leads to poorer resolution of ^{55}Mn hyperfine structure than typically observed in more strongly exchange-coupled Mn(III)Mn(IV) systems.[2,6] Zheng *et al.*[33] attribute such a CW-EPR spectrum to an antiferromagnetically exchange-coupled Mn(III)Mn(IV) system where the exchange coupling is weak compared to the zero-field splitting (ZFS) of the isolated ions and where additional terms are needed to adequately describe the effective hyperfine matrix. The EPR spectrum depends on the effective hyperfine interaction matrix ($\tilde{\mathbf{A}}$) for each Mn nucleus which is related to the isolated ion hyperfine interaction matrix ($\tilde{\mathbf{a}}$) and the ratio of the isolated ion ZFS D parameter to the exchange coupling constant (J)[33,56−58]

(67) Caudle, M. T.; Riggs-Gelasco, P.; Gelasco, A. K.; Penner-Hahn, J. E.; Pecoraro, V. L. *Inorg. Chem.* **1996**, *35*, 3577−3587.
(68) Sturgeon, B. E.; Britt, R. D. *Rev. Sci. Instrum.* **1992**, *63*, 2187−2192.
(69) Davies, E. R. *Phys. Lett.* **1974**, *47A*, 1−2.
(70) Mims, W. B.; Peisach, J. In *Biological Magnetic Resonance*; Berliner, L. J., Ruben, J., Eds.; Plenum Press: New York, 1981; pp 213−263.
(71) Mims, W. B. *J. Magn. Reson.* **1984**, *59*, 291−306.
(72) Caudle, M. T.; Pecoraro, V. L. *J. Am. Chem. Soc*, in press.
(73) Hsieh, W.; Caudle, M. T.; Pecoraro, V. L. Unpublished results.

$$\tilde{\mathbf{A}}_{\mathbf{III}} = +2\tilde{\mathbf{a}}_{\mathbf{III}} + \frac{2\tilde{\mathbf{a}}_{\mathbf{III}}}{5\,J}(7\tilde{\mathbf{D}}_{\mathbf{III}} + 2\tilde{\mathbf{D}}_{\mathbf{IV}}) \quad (7)$$

$$\tilde{\mathbf{A}}_{\mathbf{IV}} = -1\tilde{\mathbf{a}}_{\mathbf{IV}} - \frac{2\tilde{\mathbf{a}}_{\mathbf{IV}}}{5\,J}(7\tilde{\mathbf{D}}_{\mathbf{III}} + 2\tilde{\mathbf{D}}_{\mathbf{IV}}) \quad (8)$$

where $\tilde{\mathbf{D}}$ is the 3 × 3 ZFS matrix whose magnitude depends only on the scalar D value ($\tilde{\mathbf{D}} = (D/3)\cdot\tilde{\Delta}$) when the rhombic ZFS E parameter is zero. Due to the high symmetry around an isolated Mn(IV) ion, its ZFS D parameter is assumed to be 0. Assuming that the isolated Mn(III) D values are comparable in μ-oxo and μ-alkoxo bridged species, the ≥10-fold smaller J value in the μ-alkoxo bridged systems alters the effective hyperfine interactions and leads to different (∼12-line) EPR spectra than observed for the μ-oxo bridged systems. In the μ-oxo bridged systems, terms in D/J are effectively ignored due to the larger J values.[33] The large D/J ratio observed in the 2-OH-SALPN ligated Mn(III)Mn(IV) complexes studied here profoundly affects the effective ^{55}Mn hyperfine tensors ($\tilde{\mathbf{A}}$): the anisotropic ZFS tensor for isolated Mn(III) contributes significant anisotropy to the effective hyperfine interactions of both Mn(III) and Mn(IV).[33]

ESE-ENDOR. Water Ligation. Davies ^{1}H ENDOR spectra of **1** + ^1H_2O and **1** + ^2H_2O are presented in Figure 3. The position in the ESE-EPR envelope where the ENDOR experiment was performed (4250 G) is indicated in the inset. The ENDOR transitions marked with ¶ and § do not track as protons with magnetic field (not shown) and are assigned to other magnetic nuclei in the complex, possibly ^{14}N, ^{35}Cl/^{37}Cl, and/or ^{55}Mn. The ENDOR spectra of the + ^1H_2O and + ^2H_2O complexes are similar and include hyperfine couplings to protons in the 2-OH-3,5-Cl_2-SALPN ligand. Hyperfine coupling values for these protons are given in Table 1. Of particular interest are hyperfine parameters for the protons of the water ligated to the Mn(III)Mn(IV) complex. ^{1}H ENDOR resonances attributable to ligated water protons disappear upon deuteration: ENDOR features are absent in the + ^2H_2O ligated complex at frequencies of $\nu^1_H \pm 8.8$ MHz, $\nu^1_H \pm 3.8$ MHz, and $\nu^1_H \pm 2.3$ MHz. The $^1H_2O - {}^2H_2O$ subtraction spectrum shows the ENDOR signature of the protons of the ligated water.[74]

Our assignment of the ENDOR spectral features for the two ligated water protons uses a pair of inequivalent axial hyperfine interactions. We have also considered an alternative assignment to a single rhombic hyperfine interaction from spectrally equivalent protons, but we eliminate this possibility since both OH^- and methanol ligated complexes show only a single peak in this region (*vide infra*) and the fact that metrical parameters which would give the required rhombic spectrum are physically inconsistent with the known binding mode for these ligands (*vide infra*). In a weakly hyperfine-coupled $S = 1/2$, $I = 1/2$ system ($g\beta B/A \geq 40$),[75] a first order perturbation theory analysis predicts symmetrically placed ENDOR transition frequencies at[64]

$$\nu_{\mathrm{ENDOR}} = |\nu_N + m_S A| \quad (9)$$

where ν_N is the Larmor frequency and equals $g_N\beta_N B$, and $m_S = +1/2$ or $-1/2$. The hyperfine term is $A = A_{\mathrm{iso}} + T_{\mathrm{dip}}(3\cos^2\theta - 1)$,[64] where θ is the angle between the vector connecting the electron and nuclear spin and the static external magnetic field. For our frozen glass samples, θ ranges from 0° to 90°, and equation 9 describes the overlapping ENDOR "powder patterns," symmetric about the Larmor frequency ν_N for each proton, which are plotted in Figure 3.[76] The more intense features observed at $\nu^1_H \pm 3.8$ MHz and $\nu^1_H \pm 2.3$ MHz in the powder patterns for the two inequivalent protons are from complexes oriented such that $\theta = 90°$. The intensity decreases monotonically to $\nu^1_H \pm 8.8$ MHz corresponding to molecules oriented such that $\theta = 0°$, where no differences are resolved between the spectral patterns assigned to inequivalent protons.[77]

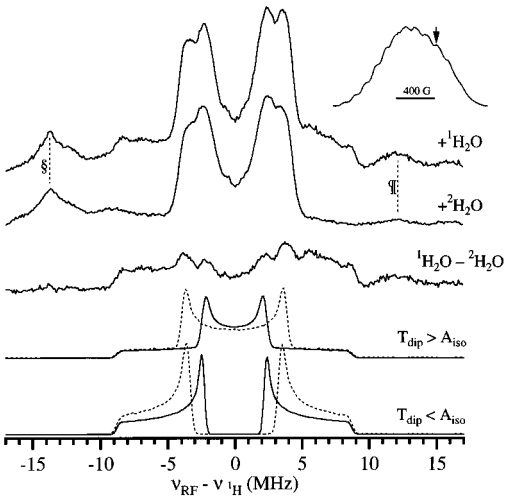

Figure 3. Davies ^{1}H ENDOR spectra of **1** with ^1H_2O and ^2H_2O ligated to Mn(III). An $^1H_2O - {}^2H_2O$ ENDOR difference spectrum is so labeled. Simulations of the ENDOR patterns expected from the two hyperfine parameter sets (large vs small T_{dip}), each with inequivalent proton hyperfine couplings, are shown. The field at which ENDOR is performed is marked on the ESE-EPR spectrum in the inset. Experimental parameters: $\nu_{MW} = 10.762$ GHz; $B = 4250$ G; $\tau = 400$ ns; $\pi/2 = 25$ ns; MW power ≈ 20 W; RF pulse = 8 μ s; RF power ≈ 1 kW; repetition rate = 500 Hz; temperature = 4.2 K.

Table 1. ^{1}H Hyperfine Coupling Constants (MHz) Observed in Solvent Ligated (2-OH-SALPN)$_2$Mn(III, IV) Systems

+ Water	+ Methanol
Not Isotopically Exchanged	
0.3(?)	0.35
1.0	1.0
1.4	1.4
	2.45
4.7	5.0
6.8	6.4
Isotopically Exchangeable "OH" Protons	
17.6 ($A_\parallel$)	17.6 ($A_\parallel$)
6.6 ($A_\perp$)	6.4 ($A_\perp$)
17.6 ($A_\perp$)	
4.6 ($A_\perp$)	
Methyl Protons, $A_{iso} = 0$	
	2.2 (T_{dip})
	3.6 (T_{dip})
	5.7 (T_{dip})

(74) While the ENDOR response may be somewhat nonlinear, the ^{1}H ENDOR signal that obviously disappears in the $A_\parallel$ region upon ^2H_2O subsitution must be from protons in ligated ^1H_2O. The ENDOR spectra of the ^1H_2O and ^2H_2O samples are subtly, but definitely, distinct in the $A_\perp$ region as well. We present the data as a subtraction spectrum to emphasize the lineshape differences. Such a subtraction is valid since any nonlinearities in the ^{1}H ENDOR response should be identical in the $A_\perp$ region of the $+^1H_2O$ and + ^2H_2O spectra and will not contribute to the subtraction spectrum. Finally, the ESEEM technique (*vide infra*) provides an independent measure of T_{dip}, which is consistent with our interpretation of the subtracted ENDOR lineshape.

(75) Sturgeon, B. E.; Ball, J. A.; Randall, D. W.; Britt, R. D. *J. Phys. Chem.* **1994**, *98*, 12871−12883.

(76) This is for the case where the nuclear Zeeman interaction dominates ($A \leq \nu_N$).

(77) The intensities of the perpendicular turning points are less than shown in the simulations. However, the conditions under which the experiment was performed (relatively short microwave pulses), transition intensities are reduced near the proton Larmor frequency (Doan, P. E.; Fan, C.; Davoust, C. E.; Hoffman, B. M. *J. Magn. Reson.* **1991**, *95*, 196−200, and ref 61) where the perpendicular turning points are expected.

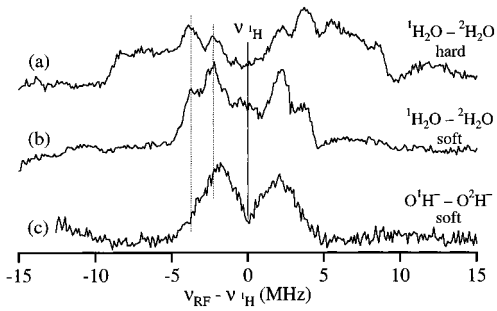

Figure 4. ENDOR difference spectra (^{1}H−^{2}H) for water and hydroxide ligated to **1**. Trace a is the difference spectrum for water ligated to **1** recorded using short, high-power microwave pulses (from Figure 3). Trace b is the difference spectrum for the same complex but recorded using longer, lower-power microwave pulses. Trace c is the difference spectrum for hydroxide ligated to **1** recorded using longer, lower-power microwave pulses. Experimental parameters (traces b and c): ν_{MW} = 10.000 GHz (water), 10.062 (MeOH); B = 3775 G (water), 3880 G (MeOH); τ = 350 ns; $\pi/2$ = 100 ns; MW power ≈ 1 W; RF pulse = 8 μs; RF power ≈ 1 kW; repetition rate = 500 Hz; temperature = 4.2 K.

The inequivalence of the water protons is confirmed by comparing isotopic subtraction spectra (protons − deuterons) from complexes where either water or hydroxide are ligated to **1** (Figure 4). The two lower traces in Figure 4 were performed using longer microwave pulses. Such "soft" microwave excitation accentuates the weakly coupled portion ($\nu^1_H \pm \sim 5$ MHz) of the spectrum. The two intense features at $\nu^1_H \pm 3.8$ MHz and $\nu^1_H \pm 2.3$ MHz are present in the ENDOR spectra of **1** + H_2O obtained with both short (hard) and long (soft) microwave pulse conditions (traces a and b). While these $^1H_2O^- - {}^2H_2O$ subtraction spectra exhibit two peaks in this spectral region from the two water protons,[78] the $O^1H^- - O^2H^-$ subtraction shows only a single set of peaks at $\nu^1_H \pm 1.9$ MHz, corresponding to the single hydroxide proton. The hydroxide ligated subtraction shows no evidence of rhombic character (*vide infra*) to the hyperfine interaction. The splitting of the peak for the hydroxide ligated complex is less than either splitting in the water ligated complex.

Though in general a rhombic pattern is expected for protons coupled to a spin-exchanged metal cluster as reported by Khangulov *et al.*[40] and DeRose *et al.*[56] (see Appendix also), spectra which appear axial are observed for the isotopically exchangeable water protons in this system. The pairwise splittings between the prominent features in each ENDOR powder pattern are designated $A_\perp$ (θ = 90°) and $A_\parallel$ (θ = 0°), and these terms are related to T_{dip} and A_{iso}: $T_{dip} = A^d_{xx} = (A_\parallel - A_\perp)/3$ and A_{iso} = trace{$\tilde{\mathbf{A}}$} = $(A_\parallel + 2A_\perp)/3$. The entire ^{1}H ENDOR powder pattern is observed in these samples due to the selection of the full range of angles within several ^{55}Mn EPR hyperfine powder patterns. The ENDOR turning points due to the bound water proton exhibiting the $\nu^1_H \pm 3.8$ MHz and $\nu^1_H \pm 8.8$ MHz features can be analyzed assuming one of the two possible hyperfine patterns shown in dashed lines simulated at the bottom of Figure 3. The simulations differ in the relative signs of $A_\parallel$ and $A_\perp$: opposite signs give a largely dipolar parameter set ($T_{dip} = \pm 8.4$ MHz, $A_{iso} = \mp 0.8$ MHz), while identical signs give a largely isotropic parameter set ($T_{dip} = \pm 3.3$ MHz, $A_{iso} = \mp 10.9$ MHz). Similarly, the ENDOR features of the other water proton give either $T_{dip} = \pm 7.4$ MHz, $A_{iso} = \mp 2.8$ MHz for oppositely signed $A_\parallel$ and $A_\perp$and $T_{dip} = \pm 4.3$ MHz, $A_{iso} = \mp 8.9$ MHz for $A_\parallel$ and $A_\perp$ of the same sign. ENDOR cannot easily determine the magnitude of dipolar interaction, since the spectral region in which the spectra are most different, the region immediately surrounding the Larmor frequency, suffers from spectral interference from the more weakly coupled ligand backbone protons. Suppression of ENDOR intensity in this region in the Davies ENDOR sequence further complicates the matter.

Fortunately, two pulse ESEEM spectroscopy can be used to independently determine the dipolar part of the hyperfine interaction for an $S = 1/2$, $I = 1/2$ spin system.[79,80] We have thus employed ESEEM to determine which hyperfine parameter set is appropriate for water bound to the Mn(III)Mn(IV) complex. A two-pulse ESEEM pattern follows the form[81]

$$V(\tau) = 1 - \frac{k}{2}\left\{1 - [\cos(\omega_\alpha\tau) - \cos(\omega_\beta\tau)] + \frac{1}{2}[\cos(\omega_+\tau) + \cos(\omega_-\tau)]\right\} \quad (10)$$

where

$$\omega^\alpha_\beta = 2\pi\nu^\alpha_\beta = 2\pi[(\pm A/2 - \nu_N)^2 + B^2/4]^{1/2}$$
$$A = A_{iso} + T_{dip}(3\cos^2\theta - 1)$$
$$B = 3T_{dip}\cos\theta\sin\theta \quad (10a)$$
$$k = \left(\frac{\nu_N B}{\nu_\alpha \nu_\beta}\right)^2$$
$$\omega_\pm = \omega_\alpha \pm \omega_\beta$$

Equation 10 predicts modulation at the nuclear precession frequencies of the coupled nuclei (ν^α_β) and inverted modulation at their sum and difference frequencies ($\nu_\pm$). For a relatively large nuclear Zeeman component ($|T_{dip} + 2A_{iso}| \ll 4\nu_N$), the $\omega_\pm$ modulation components will present inverted features at frequencies of ∼0 and $\sim 2\nu_N$ which are particularly sensitive to the dipolar hyperfine interaction (T_{dip}).[79]

Time domain two-pulse ESEEM patterns for the ^1H_2O and ^2H_2O ligated complexes are presented in Figure 5, panel A. The two-pulse echo decays over the relatively short phase memory time ($\sim T_2$), causing the modulation to damp out in less than 3.2 μs. The frequency domain spectra obtained from Fourier analysis[71] of these modulation patterns are presented in panel B. In the $^+{}^1H_2O$ ligated complex spectrally isolated features are observed at $\sim\nu^1_H$ and $\sim 2\nu^1_H$, while a complex frequency spectrum due to ^{14}N is observed at lower frequency (≤8 MHz).[82] These features, in addition to ^{2}H resonances at $\sim\nu^2_H$ and $\sim 2\nu^2_H$, appear in the $^+{}^2H_2O$ ligated complex. The ^{1}H feature at $\sim 2\nu^1_H$ in the ^1H_2O ligated complex is particularly useful in determining the magnitude of the dipolar interaction, $|T_{dip}|$.[79] In addition to the large inverted feature at precisely $2\nu^1_H$ due to numerous weakly coupled protons, a smaller feature ($\nu_\alpha + \nu_\beta$) from strongly dipolar coupled protons is present at a frequency

(78) In a rhombic interpretation of the ENDOR spectrum, the peaks at $\nu^1_H \pm 3.8$ MHz in the $^1H_2O-{}^2H_2O$ subtraction spectrum would be rhombic shoulders. On the contrary, these spectral features in short (hard) microwave excitation subtraction spectrum (Figure 4, trace a) appear to be peaks, showing little resemblance to rhombic shoulders.

(79) Reijerse, E. J.; Dikanov, S. A. *J. Chem. Phys.* **1991**, *95*, 836−845.
(80) Lai, A.; Flanagan, H. L.; Singel, D. J. *J. Chem. Phys.* **1988**, *89*, 7161−7166.
(81) Mims, W. B. *Phys. Rev. B* **1972**, *5*, 2409−2419.
(82) In this system, the nitrogen hyperfine does not meet "exact field cancellation conditions", which would lead to sharp ^{14}N ESEEM transitions when the nitrogen hyperfine is largely isotropic and $A^{14}_N/2 = \nu^{14}_N$. Further analysis of the ^{14}N ESEEM is outside the focus of this paper.
(83) Since the exact shift in ($\nu_\alpha + \nu_\beta$) depends on the complex line shape of this ESEEM peak, the values determined from the ENDOR data are preferred.

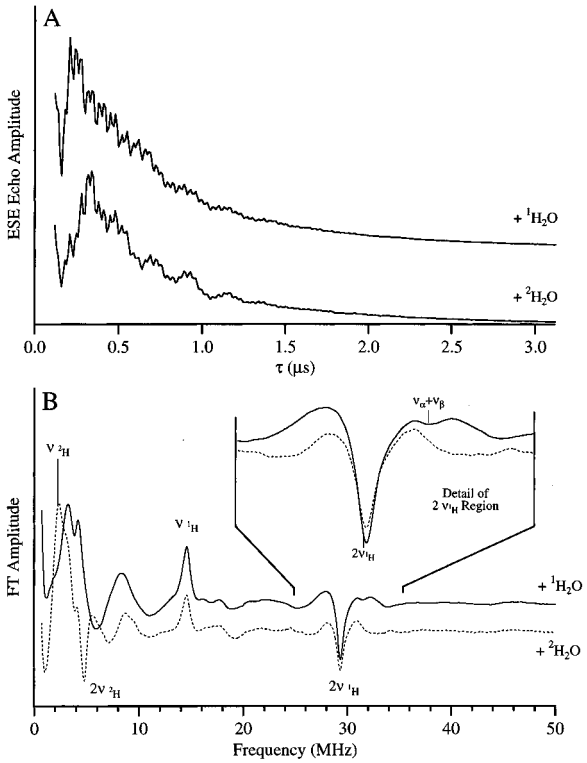

Figure 5. Time domain (panel A) and frequency domain (panel B) two pulse ESEEM of **1** ligated by ^1H_2O and ^2H_2O. ^1H and ^2H Larmor frequencies and combination features are marked. The inset shows an expanded view of the ^1H $\nu_\alpha + \nu_\beta$ region from which the magnitude of the dipolar interaction of the bound water can be determined. Experimental parameters: $\nu_{MW} = 10.228$ GHz; $B = 3437$ G; starting $\tau = 120$ ns; $\pi/2 = 15$ ns; MW power ≈ 50 W; repetition rate $= 500$ Hz; temperature $= 4.2$ K.

slightly higher than $2\nu_{^1H}$. The magnitude of the shift is directly related to T_{dip}:[79]

$$\delta = (\nu_\alpha + \nu_\beta) - 2\nu_N = \frac{9}{16}\frac{(T_{dip})^2}{\nu_N} \qquad (11)$$

An expanded plot of the $2\nu_{^1H}$ region for the $+^1H_2O$ and $+^2H_2O$ samples is included as an inset of Figure 5B. The $+^1H_2O$ ligated complex shows an inverted feature 2.33 MHz above $2\nu_{^1H}$ (marked $\nu_\alpha + \nu_\beta$ in Figure 5B) which disappears upon deuteration. According to this equation, this 2.33 MHz shift is due to a dipolar interaction ($|T_{dip}|$) of approximately 7.8 MHz. Similar dipolar shifts in the $\nu_\alpha + \nu_\beta$ ESEEM feature consistent with a large $|T_{dip}|$ are observed across the EPR envelope, as demonstrated Figure 6. The average $|T_{dip}|$ value for five points across the envelope is 7.7 MHz ± 0.1 MHz. This is between the 7.4 and 8.4 MHz values of $|T_{dip}|$ from the strongly dipolar coupled ENDOR parameter sets for the two water protons.[83] The magnitude of T_{dip} determined using equation 11 is completely independent of the values determined from the ENDOR pattern in Figure 3. We thus conclude that the strongly dipolar coupled parameter set (Table 1) is the correct one for describing water bound to the Mn(III) ion in this system.

With the magnitude of the dipolar coupling determined, the position of the protons on the ligated water with respect to the Mn(III) nucleus can be established. A simple radially symmetric point dipole approximation (equation 5) is inappropriate for this system. For multinuclear metal clusters it is important to consider the effects of electron spin density distributed among the metal ions.[16, 39,40,56] For the model used here,[16,39,40,56] a proton experiences a dipolar interaction with each Mn ion of

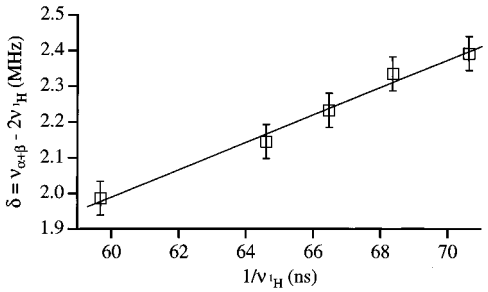

Figure 6. Graph showing the dipolar-induced shift from $2\nu_{^1H}$ (δ) in two pulse ESEEM spectra across the EPR envelope of **1** + ^1H_2O. The error bars correspond to the digital resolution of the ESEEM spectra. The magnetic fields are 3327 G, 3437 G, 3535 G, 3637 G, 3937 G; other experimental conditions in Figure 5.

the exchange coupled manganese complex: the dipolar interactions with the Mn(IV) ion and the Mn(III) ion contribute additively to the observed dipolar hyperfine interaction

$$\tilde{\mathbf{A}}_{dip} = p_{Mn(III)}\,\tilde{\mathbf{A}}'_{Mn(III),dip} + p_{Mn(IV)}\,\tilde{\mathbf{A}}'_{Mn(IV),dip} \qquad (12)$$

where the primes emphasize that the addition is performed in a common axis system, and $\tilde{\mathbf{A}}_{q,dip}$ was defined in equation 5. In general, the individual dipolar hyperfine interactions have distinct principal axis systems, and a matrix rotation (unitary transform) is required to bring them into the same axis system before the addition (see appendix). The p_q terms are quantum mechanical "projection factors" which are a consequence of converting from an uncoupled basis set to a coupled basis set. The projection factors are dependent on the electronic spin, S_q, of the isolated ions: $p_q = \langle S', m_{S'}; S'_1, S'_2|\hat{\tilde{S}}_T \cdot \hat{\tilde{S}}_q/\hat{\tilde{S}}_T{}^2|S, m_S; S_1,S_2\rangle$ (see Appendix). Consequently, the projection factors depend on the oxidation states of the isolated ions as well as whether they are high or low spin. For high spin, Mn(III) $p_{Mn(III)} = +2$, and for Mn(IV), $p_{Mn(IV)} = -1$.[21,32,33] In this model, the dipolar field experienced by the proton arises from its interaction with two nearby metal centers that are both treated as point dipoles dependent upon the projection factors. For extremely short Mn−H distances, the point dipole approximation breaks down because the unpaired electron resides in radially diffuse *d*-orbitals. This model would also be inappropriate if significant charge were delocalized onto the ligands and/or bridging groups. Neither of these limiting conditions is met, and therefore this model represents this system well.

The relative geometry of a generalized water proton and the Mn(III) and Mn(IV) ions is defined in the inset to Figure 7. The proton experiences a dipolar interaction which depends on the Mn(III)−H radial distance (r_A) and the Mn(IV)−H radial distance (r_B). The matrix rotations required for the addition in equation 12 may introduce rhombicity into the total dipolar hyperfine interaction ($\tilde{\mathbf{A}}_{dip}$). The principal components of the resulting hyperfine interaction can be determined analytically (see appendix):

$$A'_x = \frac{1}{2}(2T_A - T_B - 3\Gamma) \qquad (13a)$$

$$A'_y = -(2T_A - T_B) \qquad (13b)$$

$$A'_z = \frac{1}{2}(2T_A - T_B - 3\Gamma) \qquad (13c)$$

where

$$\Gamma = [4T_A{}^2 + T_B{}^2 - 4T_A T_B \cos(2\alpha + 2\beta)]^{1/2} \qquad (13d)$$

These equations allow us to examine the dependence of r_A and

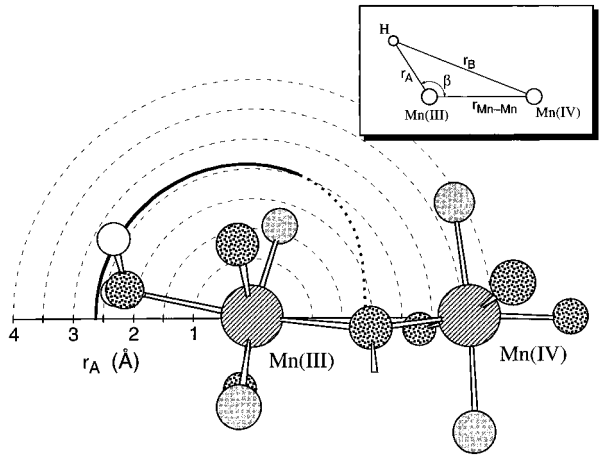

Figure 7. Polar plot showing the contour where the intermediate hyperfine value, A_y, is held constant at 8.4 MHz. Superimposed on the polar plot is a model showing water bound to the complex. The model is based on the ENDOR and ESEEM results and the crystal structure of the THF adduct. The two Mn atoms and the water proton lie in the plane of the page. The inset shows the schematic representation of the geometry of Mn(IV), Mn(III), and a water proton. The dotted portion of the trace indicates where the rhombicity χ is greater than 0.2.

β on any component of the hyperfine interaction matrix. For comparison with the ENDOR data, we choose to follow a contour of constant A_y, since this feature has maximum ENDOR intensity in a rhombic powder pattern. The solid and dotted portion of the polar plot in Figure 7 shows where the the hyperfine interaction component A_y is constant at 8.4 MHz (A_x and A_z are unrestricted). The solid trace in Figure 7 shows the region where the rhombicity, χ, of the hyperfine interaction (*vide infra*) is small, such as in the observed spectra, $\chi = (A_x - A_y)/A_z \leq 0.2$, while the dotted portion of the trace shows where the polar parameters (r_A, β) give a hyperfine interaction which is more rhombic than observed. All such contours are axially symmetric about the Mn(III)−Mn(IV) axis. Little angular dependence is observed in the radial distance for $\beta > 120°$ in the T_{dip} 8.4 MHz contour shown in Figure 7. The opposite signs of the projection factors for Mn(III) and Mn(IV) give opposing dipolar fields, which tend to cancel each other in the region between the Mn nuclei. Thus, A_y is held constant by moving the proton closer to the Mn(III) nucleus in the region between nuclei (small β) than in the end regions (large β). This is exemplified in the values of r_A obtained by setting equation 13b for the A_y component equal to 8.4 MHz at the possible extremes for β : for $\beta = 180°$, $r_A = 2.63$ Å; while at 0°, where the proton is between Mn ions, r_A is 1.90.

The value of 8.4 MHz for A_y was chosen since this value of T_{dip} was determined from the ENDOR data for one of the water protons. The ENDOR spectra we observe for this system are axial in appearance. The rhombic hyperfine parameters for this system at large angle β (i.e., $\beta > 90°$) show small rhombicity, $\chi \leq 0.2$. The finite line width of the ENDOR transitions makes a purely axial ENDOR spectrum ($\chi = 0$) indistinguishable from a slightly rhombic one ($\chi \leq 0.2$). For instance, at $\beta = 90°$ the rhombicity is less than 0.2, and it decreases in a sharp monotonic manner for larger angles. Thus, the axial appearance of the ENDOR transitions for ^1H_2O ligated to **1** constrains the angle β to be greater than ~90°. The A_z component of the dipolar interaction is spectrally separated from A_x and A_y, and it also depends on the angle β: for $\beta > 135°$ an insignificant difference of ≤0.2 MHz is observed between experimental and calculated values. Thus, the observed parallel turning point (A_z) further limits β to be greater than 135°. The analogous plot for the other water proton ($T_{dip} \approx 7.4$ MHz) shows similar features.

Overlaid on the contour plot (at the same scale) is a model of the water bound μ-alkoxo bridged Mn(III)Mn(IV) system. The two Mn nuclei and one water proton define the plane of the page (in the view shown, the other water proton is mostly hidden behind the water oxygen). This molecular skeleton is based on the radial distance and orientation of the ligated water (determined above) and the crystallographically characterized THF complex of **1**.[53] In the water bound model depicted in Figure 7, the Mn(III)−Mn(IV) distance is fixed at 3.65 Å, the same as observed in the THF ligated crystal structure. The bond lengths and bond angles around both Mn(III) and Mn(IV) are assumed to be identical with those in the THF bound structure, except for the Mn(III)−O(water) bond length, λ. The water orientation shown is not uniquely determined by the techniques used here, which are primarily sensitive to Mn(III)−H radial distances: the Mn(III)−H radial distance is determined by the bond length λ as well as the angle (ζ) which H−O−H plane makes with this bond. In the model shown the angle ζ is 120°, and the bond length λ is 2.20 Å. These values of λ and ζ were chosen because they represent a reasonable compromise between the angle ζ in the limit of sp^3 hybridization for O(water) and the Mn(III)−O(water) distance, λ, observed in other complexes where water binds along the Jahn−Teller axis.[84] Increasing the angle ζ further shortens the bond length λ to unreasonably short distances. The bond length λ is 0.1 Å shorter in this water ligated model than the THF ligated structure.[53] Reduced steric hindrance of water compared to THF may allow water to get closer to the Mn(III) ion. Torsion of water about the Mn(III)−O axis is not specified by the experimentally determined T_{dip}: the Mn(III)−H distance shows little dependence on the torsional angle for large β. Thus, a model for the water bound complex can be constructed from the ENDOR and ESEEM data.

Above we discounted a rhombic origin for the protons of ligated water based on the appearance of the $^1H_2O-^2H_2O$ ENDOR spectrum in Figure 3. Using eqs 13, a rhombic interpretation of the data can independently be eliminated based on the contradiction between the known binding mode of solvent-ligands to the Mn(III)Mn(IV) core and the geometry defined by the metrical parameters r_A and β that would give a rhombic spectrum for equivalent protons matching that in Figure 3. Such a rhombic hyperfine interaction (isotropic + dipolar) would have components of [−4.6, −7.6, +17.6] MHz. For this rhombic parameter set, the value of A_{iso} is +1.8 MHz and the principal components of $\tilde{\mathbf{A}}_{dip}$ are [−6.4, −9.4, +15.8] MHz. A numerical evaluation of the dipolar hyperfine interaction components for the entire r_A, β parameter space indicates that parameters of $r_A \approx 2.745$ Å and $\beta \approx 76°$ give this dipolar hyperfine interaction. While this value of r_A is reasonable, a β of 76° is entirely inconsistent with water ligation in the known binding motif roughly along the Mn(III)−Mn(IV) axis. It is clear that this rhombic interpretation of the ENDOR spectra is unfounded, based on the sum of three individually convincing arguments: the single peak in the OH^- spectrum (*vide supra*), the axial lineshape of the $^1H_2O - {}^2H_2O$ subtraction spectrum (*vide supra*), and the physically inconsistent binding mode predicted by the metrical parameters required to give a rhombic powder pattern.

The ^1H ENDOR and ESEEM results obtained on water bound to a Mn(III)Mn(IV) dinuclear complex can be compared to those obtained on the $[Mn(H_2O)_6]^{2+}$ complex, which has been analyzed in both an aqueous glass[85,86] and in a magnetically

(84) Mikuriya, M.; Yamato, Y.; Tokii, T. *Bull. Chem. Soc. Jpn.* **1992**, *65*, 1466−1468.
(85) Sivaraja, M.; Stouch, T.; Dismukes, G. *J. Am. Chem. Soc.* **1992**, *114*, 9600−9603.

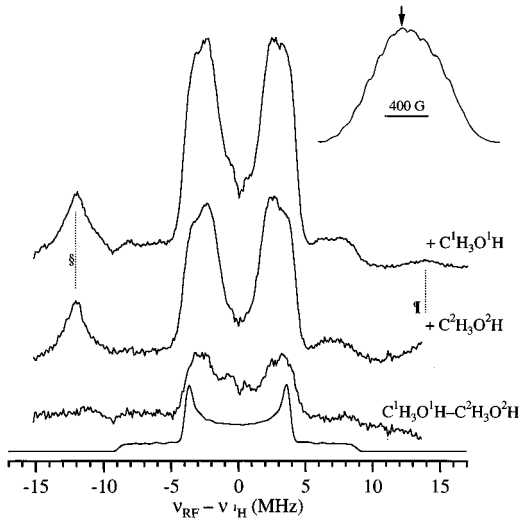

Figure 8. Davies ^{1}H ENDOR of $C^2H_3O^2H$ and $C^1H_3O^1H$ ligated to **1**, the ENDOR difference spectrum, and simulation of the powder pattern due to the alcohol proton. The trace labels indicate the isotopic composition of the ligated methanol. The inset shows the position in the EPR envelope where ENDOR was performed. Experimental Davies parameters: $\nu_{MW} = 10.5022$ GHz; $B = 3830$ G; $\tau = 410$ ns; $\pi/2 = 25$ ns; MW power ≈ 20 W; RF pulse $= 8\ \mu$s; RF power ≈ 1 kW; repetition rate $= 500$ Hz; temperature $= 4.2$ K.

dilute crystalline lattice.[87] Both $[Mn(H_2O)_6]^{2+}$ systems exhibit largely dipolar hyperfine interactions, as observed for water ligated to **1**. In the crystalline work, $Mn^{2+}-H$ radial distances determined from crystallography compared favorably (± 0.1 Å) with those determined from a point-dipole analysis (equation 5). In both $[Mn(H_2O)_6]^{2+}$ systems, radial distances of ~ 2.85 Å are observed, which is 0.1−0.2 Å longer than the Mn(III)−H radial distance observed in **1** + ^1H_2O. A slightly shorter Mn−H distance in the latter system is expected since Mn−O(water) bond distances tend to be shorter for Mn(III) than for Mn^{2+}, shortening the Mn−H distance. In single crystal studies of $[Mn(H_2O)_6]^{2+}$, de Beer *et al.*[87] observed an isotropic hyperfine (A_{iso}) of ~ 0.9 MHz. For a frozen glass sample of $[Mn(H_2O)_6]^{2+}$, Tan *et al.*[86] report an A_{iso} of 0.9 ± 0.1 MHz, while Sivaraja *et al.*[85] report an A_{iso} of 0.8 ± 0.3 MHz. The 0.9 MHz A_{iso} of one of the terminally bound water protons in this dinuclear Mn system correlates well with these values, while the 2.7 MHz value is somewhat higher.

Methanol Ligation. The CW-EPR spectrum of **1** + MeOH is included in the Figure 2. The Davies ENDOR of **1** ligated with $C^1H_3O^1H$ and $C^2H_3O^2H$ is presented in Figure 8. A $C^1H_3O^1H-C^2H_3O^2H$ difference spectrum is shown. The difference trace resembles that observed for water: a peak at $\nu^1_H \pm 8.8$ MHz disappears upon deuteration. With the single alcohol proton, however, only a single perpendicular turning point is observed at $\nu^1_H \pm 3.8$ MHz. Ensuring that the difference is indeed from the alcohol proton, the $\nu^1_H \pm 8.8$ MHz parallel turning point and $\nu^1_H \pm 3.8$ MHz perpendicular turning point disappear in the $C^1H_3O^2H$ ligated complex (not shown). Therefore, it appears that the alcohol proton in methanol assumes a similar orientation with respect to the Mn complex as the water proton, which has a large T_{dip} interaction with a radial distance of ~ 2.65. The simulation shown beneath the subtraction uses the strongly dipolar coupled parameter set from the water ligated complex. In addition to the ENDOR signature of the exchangeable deuteron, the difference trace exhibits contributions from the methyl deuterons. In comparison with the water subtraction trace, there is more intensity at $\nu^1_H \pm 3.0$ MHz. The alcohol proton contributes a portion of this intensity, but some intensity is due to methyl protons. Matrix-suppression effects in the Davies sequence (discussed above) preclude determining the significance of features at $\nu^1_H \pm \sim 0.7$ MHz in the subtracted spectrum which could be attributed to more weakly coupled methyl protons.

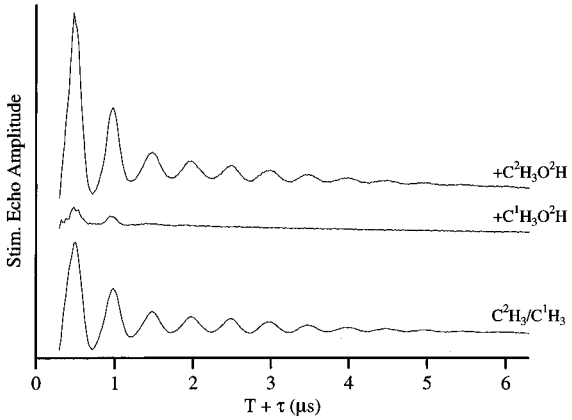

Figure 9. Three pulse ESEEM patterns of **1** ligated by $C^2H_3O^2H$ and CH_3O^2H. The ratioed trace labeled C^2H_3/CH_3 is the isolated modulation from the methyl deuterons. Experimental parameters: $\nu_{MW} = 9.26082$ GHz; $B = 3080$ G; $\tau = 229$ ns; starting $T = 71$ ns; $\pi/2 = 15$ ns; MW power ≈ 200 W; repetition rate $= 500$ Hz; temperature $= 4.2$ K.

Three pulse ^{2}H ESEEM provides an excellent method for probing Mn−^{2}H distances.[16,17] Three pulse ESEEM is preferred over two pulse ESEEM for this study since three pulse modulations decay with the longer T_1 relaxation time, which facilitates observation of multiple cycles of low frequency modulations, such as those from ^{2}H nuclei. For a negligible nuclear quadrupole interaction, which is generally a valid assumption for ^{2}H, the three pulse ESEEM modulation pattern is given by

$$V(\tau,T) = \frac{1}{2}[V_\alpha(T,\tau) + V_\beta(T,\tau)] \qquad (14)$$

where

$$V_\alpha(T,\tau) = 1 - \frac{k}{2}[1 - \cos(\omega_\alpha(\tau + T))]\sin^2\frac{\omega_\beta\tau}{2} \qquad (14a)$$

$$V_\beta(T,\tau) = 1 - \frac{k}{2}[1 - \cos(\omega_\beta(\tau + T))]\sin^2\frac{\omega_\alpha\tau}{2}$$

where $V_\alpha(T,\tau)$ and $V_\beta(T,\tau)$ represent the contributions to the modulation pattern from each electron spin manifold. Three pulse modulation patterns for **1** + $C^2H_3O^2H$ and **1** + $C^1H_3O^2H$ are shown in Figure 9. The depth of the modulation is much greater for the **1** + $C^2H_3O^2H$ complex due to the greater number of coupled deuterons and the strength of their interactions. The observed modulation function is the sum of the product of modulation patterns in the two electron spin manifolds:

$$V(T,\tau) = \frac{1}{2}\left[\prod_i V_{\alpha,i}(T,\tau) + \prod_i V_{\beta,i}(T,\tau)\right] \qquad (15)$$

In the limit of weak isotropic hyperfine interactions, which will be the case for methyl deuterons, the modulations from each spin manifold will be equal ($V_\alpha(T,\tau) \approx V_\beta(T,\tau)$) and the modulation function $V(T,\tau)$ can be approximated by applying the sum before the product:

(86) Tan, X.; Bernardo, M.; Thomann, H.; Scholes, C. P. *J. Chem. Phys.* **1993**, *98*, 5147−5157.

(87) de Beer, R.; de Boer, W.; van't Hoff, C. A.; van Ormondt, D. *Acta Crystallogr. B* **1973**, *29*, 1473−1480.

$$V(T,\tau) \approx \prod_i V_i(T, \tau) \qquad (16)$$

In this limit, the modulation pattern of methyl deuterons can be isolated by ratioing the modulation pattern[88−90] from the **1** + $C^2H_3O^2H$ complex to that of the **1** + $C^1H_3O^2H$ complex, as displayed in trace c. The methyl ^2H modulation pattern is largely due to the three methyl deuterons of the bound methanol. Contributions to the modulation also arise, however, from more weakly coupled methyl deuterons of unbound solvent methanol. Modulation patterns for the ^2H nuclei can be simulated,[16,88,91] and the effective dipolar hyperfine interaction can thus be determined. Figure 10 shows such a simulation of the experimental ratioed $^2H/^1H$ trace (C^2H_3/C^1H_3) from Figure 9. The pattern was simulated with three purely dipolar deuterium interactions of (values scaled for protons in parentheses) T_{dip} = 0.337 (2.19) MHz, 0.552 (3.60) MHz, and 0.877 (5.71) MHz and a matrix contribution from 30 distant deuterons with dipolar couplings of 0.10 (0.67) MHz. The simulations include the effects of the ^2H quadrupole moment.[91] The ∼500-fold molar excess of $C^2H_3O^2H$ gives rise to these matrix deuterons.

Figure 11 depicts three contours with dipolar interactions corresponding to the three methyl deuterons (protons). These contours are calculated in an identical manner to those calculated for **1** + ^1H_2O. A structural model which is consistent with these results is overlaid on the polar plot of Figure 11. The structural model was constructed in a manner analogous to that of the water bound structure in Figure 7. The three nonequivalent Mn(III)−D(H) distances of 3.0, 3.5, and 4.0 Å are determined by the dipolar hyperfine values from the ^2H ESEEM simulation and the "spin-coupled point pair" model. Again the dotted portion of the traces show where the rhombicity χ of the hyperfine interactions is larger than 0.2. By maintaining tetrahedral angles in the methyl group the smallest H−O−C−H dihedral angle is ∼52°. Less than 0.1 Å difference is observed between modeled and experimentally determined Mn(III)−D(H) distances. Again, torsion about the Mn(III)−O bond is unspecified by the data. The alcohol proton dipolar interaction is similar to that of one water proton, requiring that they be at similar distances and orientations with respect to the Mn(III)Mn(IV) core.

Conclusions

Dipolar hyperfine interactions measured with ^1H ESEENDOR, ^1H ESEEM, and ^2H ESEEM of small molecules ligated to a μ-alkoxo bridged mixed valence Mn(III)Mn(IV) complex reveal Mn−H radial distances. The presence of electron spin density on both the Mn(III) and the Mn(IV) ions of the complex necessitates an analysis of the dipolar interactions using a model where the coupled proton experiences a point dipolar interaction with each Mn ion. Equations are presented for the components of the resulting total dipolar hyperfine interaction matrix. Using this model, analysis of the ^1H ENDOR and combination frequencies in two pulse ESEEM gives radial Mn(III)−H distances of 2.65 and 2.74 Å for protons of ligated water and a distance of 2.65 Å for the alcohol proton of ligated methanol. These protons form Mn(IV)−Mn(III)−H angles (β) that are larger than 135°. Similar analysis of three pulse ^2H ESEEM patterns from the methyl-ligated system gives Mn(III)−H distances of 3.0, 3.5, and 4.0 Å. This work provides a direct basis for analyzing water and alcohol binding to biological Mn complexes such as the tetranuclear Mn cluster of the OEC and the dinuclear Mn core of MnCat.

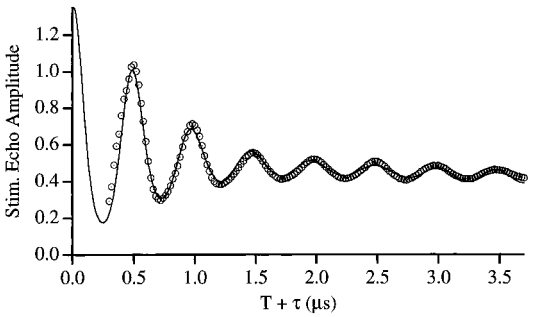

Figure 10. Experimental (circles) and simulated (solid trace) ^2H ESEEM pattern for the methyl deuterons of methanol bound to **1**. The experimental trace is the $C^2H_3C^1H_3$ ratio from Figure 9. The dipolar hyperfine parameters utilized in the simulations are given in the text. No isotropic hyperfine interactions were included in the simulation, and the ^2H quadrupolar parameters are $e^2Qq = 0.22$ MHz and $\eta = 0.1$ for each deuterium nucleus.

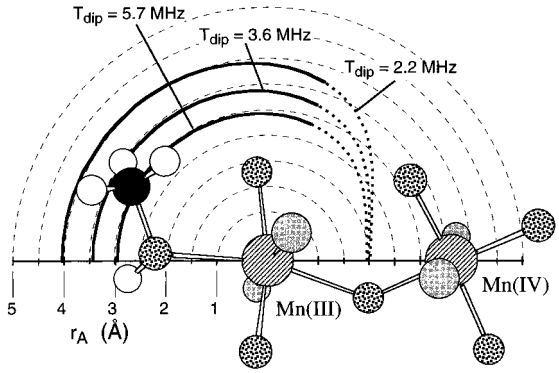

Figure 11. Polar plot obtained by maintaining A_y at constant values corresponding to the dipolar interaction for methyl deuterons with **1**. The dipolar interactions used were those obtained from the three pulse ESEEM simulation. The Mn(III) nucleus is centered at $r_A = 0$. The three traces correspond to the three methyl deuterons. The dotted portion of the trace indicates where the rhombicity, χ, is greater than 0.2.

Acknowledgment. D.W.R. acknowledges a fellowship from the University of California, Davis. V.L.P. acknowledges a grant from the National Institutes of Health (GM39406). R.D.B. acknowledges a grant from the National Institutes of Health (BMT 1 R29 GM48242-01).

Note Added in Proof. Recently Fiege *et al*. published a report on the ^1H ENDOR of the OEC.[92] In it they derive the equivalent of our eqs 13. Despite of some similarity in the notation, our equations, which are essentially identical to theirs, were derived independently.

Appendix

When considering dipolar hyperfine coupling of protons in the immediate vicinity of dinuclear metal complexes such as those of the model complex considered in this paper or in biological systems such as methane monooxygenase (MMOH), manganese catalase (MnCat), and ribonucleotide diphosphate reductase (RNR), the familiar point-dipole approximation (equation 5) breaks down.[40,56] Rather, the net dipolar interaction is

(88) Mims, W. B.; Davis, J. L.; Peisach, J. *J. Magn. Reson.* **1990**, *86*, 273−292.
(89) Warncke, K.; Babcock, G. T.; Dooley, D. M.; McGuirl, M. A.; McCracken, J. *J. Am. Chem. Soc.* **1994**, *116*, 4028−4037.
(90) Lorigan, G. A.; Britt, R. D.; Kim, J. H.; Hille, R. *Biochim. Biophys. Acta* **1994**, *1185*, 284−294.
(91) Britt, R. D.; Zimmermann, J. L.; Sauer, K.; Klein, M. P. *J. Am. Chem. Soc.* **1989**, *111*, 3522−3532.
(92) Fiege, R.; Zweygart, W.; Bittl, R.; Adir, N.; Genger, G.; Lubitz, W. *Photosyn. Res.* **1996**, *48*, 227−237.

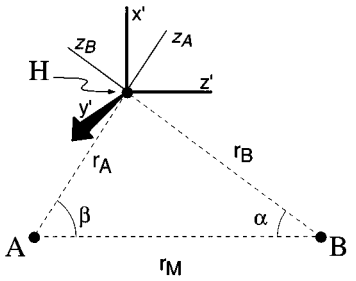

Figure 12. Geometrical representation of a proton, H, that is dipolar coupled to two exchange coupled metal atoms, A and B. The unprimed z_q axes are the unique axes in the principal axis system of the two dipolar interactions. The primed axis system is the one in which the total dipolar hyperfine is calculated.

a sum of point-dipolar interactions between the proton and metals. When there is exchange coupling between metal atoms, each dipolar hyperfine term in the sum is multiplied by the spin projection factor of the respective nucleus (equation 12). DeRose *et al.*[56] present analytical equations for the components of a dipolar hyperfine interaction where the proton forms an isosceles triangle with equidistant metal centers in mixed valence, Fe(III)Fe(II), MMOH. Khangulov *et al.*[40] use numerical methods to address the more general case of a proton oriented anywhere relative to the metal ions of superoxidized mixed valent, Mn(III)Mn(IV), MnCat. Here we follow the treatment of DeRose *et al.*[56] to extend their analytical equations for the hyperfine components in the general case of Khangulov *et al.*[40] where a proton assumes any position relative to two exchange coupled metal ions whose whose the spin projection factors are variables in the equations.

This system is parameterized by spin projection factors p_A and p_B in addition to the metrical parameters defined in Figure 12.[56] The spin projection factors are[36]

$$p_A = \frac{1}{2}\left\{1 + \frac{S_A(S_A+1) - S_B(S_B+1)}{S_T(S_T+1)}\right\} \quad \text{(A.1a)}$$

$$p_B = \frac{1}{2}\left\{1 - \frac{S_A(S_A+1) - S_B(S_B+1)}{S_T(S_T+1)}\right\} \quad \text{(A.1b)}$$

where $S_A \geq S_B$ and S_T is a member of the set $\{S_A - S_B, ..., S_A + S_B\}$. In the common situation of antiferromagnetic coupling, S_T is the first member of this set. Equation 12 gives the net dipolar hyperfine interaction matrix in a common axis system (denoted by the primes):[40,56] $\tilde{\mathbf{A}}'_{\text{dip}} = p_A\tilde{\mathbf{A}}'^{\text{dip}}_A + p_B\tilde{\mathbf{A}}'^{\text{dip}}_B$. The dipolar hyperfine interaction in its principal axis system is given by equation 5. The unique axis of the individual dipolar hyperfine interactions is along r_q, the line between metal atom q and the proton (i.e., z_A and z_B in Figure 12). Since the principal axis systems of the two dipolar interactions are only coincident for the case of $\beta = 180°$, the individual hyperfine tensors must be rotated into a common axis system before the addition indicated in equation 12 is performed. It is convenient to use a unitary transform to rotate both hyperfine interactions to a common axis system whose z' direction (the prime denoting the common axis system) is along the intermetal axis. The corresponds to a rotation of $\tilde{\mathbf{A}}^{\text{dip}}_A$ by angle $-\beta$ and a rotation of $\tilde{\mathbf{A}}^{\text{dip}}_B$ by angle $-\alpha$ (clockwise rotations correspond to negative angles), which is accomplished by use of unitary transforms (i.e., $\tilde{\mathbf{A}}'_q = \tilde{\Psi}^{\dagger}\cdot\tilde{\mathbf{A}}_q\cdot\tilde{\Psi} = \tilde{\mathbf{1}}$:[93] where the prime denotes the common axis system (the "dip" is dropped for notational convenience), $\tilde{\Psi}$ is the rotation matrix, and $\tilde{\Psi}^{\dagger}$ its transpose such that $\tilde{\Psi}^{\dagger}\cdot\tilde{\Psi} = \tilde{\mathbf{1}}$:[93]

$$\tilde{\Psi} = \begin{pmatrix} \cos\theta & 0 & \sin\theta \\ 0 & 1 & 0 \\ -\sin\theta & 0 & \cos\theta \end{pmatrix} \quad \text{(A.2)}$$

Following the rotation of each individual diagonal hyperfine interaction matrix into the common axis system (the primed axis system of Figure 12) the summation in equation 12 is performed. The resulting net dipolar hyperfine interaction matrix, $\tilde{\mathbf{A}}'_{\text{dip}}$, is nondiagonal. Diagonalization of $\tilde{\mathbf{A}}'_{\text{dip}}$ gives the principal components of the net dipolar hyperfine interaction, which is rhombic[40,56]

$$\tilde{\mathbf{A}}'_{\text{dip}} = \left[\frac{1}{2}(p_AT_A + p_BT_B - 3\Gamma),\ -(p_AT_A + p_BT_B),\ \frac{1}{2}(p_AT_A + p_BT_B + 3\Gamma)\right] \quad \text{(A.3)}$$

where

$$\Gamma = [pA^2T_A{}^2 + p_B{}^2T_B{}^2 + 2p_Ap_BT_AT_B\cos(2\alpha + 2\beta)]^{1/2} \quad \text{(A.3a)}$$

When the angle $\beta = 180°$, the Γ term equals $(p_AT_A + p_BT_B)$, giving $A'_x = A'_y$. This confirms that a purely axial spectrum is expected when the proton lies on the Mn(III)−Mn(IV) axis. These equations evaluated with $p_A = +2$ and $p_B = -1$, give eq 13.

Dipolar plots such as those in Figures 7 and 11 require these equations to be expressed as a function of a single radius (r_A) and angle (β). This can be accomplished, since the Mn(III) ion, Mn(IV) ion, and proton form the points of a triangle, and the laws of sines and cosines can be used

$$T_A = \frac{g_e\beta_e\, g_N\beta_N}{hr_A{}^3}; \quad T_B = \frac{g_e\beta_e\, g_N\beta_N}{hr_B{}^3} \quad \text{(A.4)}$$

where r_B and α are given by

$$r_B = [r_A{}^2 + r_{\text{Mn}}{}^2 - 2r_Ar_{\text{Mn}}\cos\beta]^{1/2}; \quad \alpha = \arcsin\left[\frac{r_A}{r_B}\cdot\sin\beta\right] \quad \text{(A.5)}$$

To compare with the results of DeRose *et al.*[56] on the μ-hydroxo proton which is equidistant from the Fe(II) and Fe(III) atoms in MMOH, we evaluate eq A.3 where $p_A = +7/3$, $p_B = -4/3$, $r_A = r_B = 2.5$ Å, and $\alpha = \beta = 51°$ to obtain the following for the principal components of the hyperfine tensor:

{−25.18, −4.81, 30.00} MHz

compare to {−25, −5, +30} MHz

The equations can also be evaluated using the parameters of Khangulov *et al.*[40] which were determined for an exchangeable proton in the vicinity of an exchange coupled Mn(III) Mn(IV) pair in superoxidized MnCat. For their case I(a) (Table 4)[40] $p_A = +2$, $p_B = -1$, $r_A = 3.8$ Å, $r_B = 3.9$ Å, $\alpha = 71°$ and $\beta = 67°$

{−3.72, −1.55, +5.26}MHz

compare to {−3.93, −1.73, +5.67} MHz

Altering r_A and r_B by less then 0.05 moves the agreement significantly closer.

JA963682S

(93) Zare, R. N. *Angular Momentum*; John Wiley and Sons: New York, 1988; pp 77−81.